CEAI, Vol.24, No.2, pp. 69-79, 2022 Printed in Romania

Improved BP Network-Based Sliding Mode Tracking Control for a Quadrotor UAV

Qiang-Wei Pang, De-Shi Wang, Wei Wu, Ye Chen, Yong-Yong Zhu

College of Weaponry Engineering, Naval University of Engineering, Wuhan 430000, PR China

Abstract: This paper introduces a novel trajectory tracking control method for quadrotor unmanned aerial vehicles (UAVs). In order to improve the stability of a UAV during trajectory tracking, the proposed method combined the advantages of a back propagation (BP) network and sliding mode control (SMC). A nonlinear dynamic model was first built for a quadrotor UAV by using Newton-Euler equations. The process was then divided into quasi-fully actuated and quasi-under actuated subsystems. The corresponding control law was devised with SMC. For the quasi-under actuated system, the desired roll and pitch angles were calculated according to the desired state, so as to reduce the correction error. For the quasi-fully actuated system, based on the standard BP network, the sliding mode switching function coefficient can be dynamically adjusted following the error by introducing a variable learning rate factor and a momentum factor. The simulation results show that the proposed method could accurately track the desired trajectory, and greatly suppress the chattering phenomenon with the maximum overshoot of the SMC.

Keywords: quadrotor UAV; sliding mode control; improved back propagation network; tracking control; chattering phenomenon

1. INTRODUCTION

UAVs have recently been one of the hotspots in research related to civil and military applications such as search and rescue, forest fire prevention, mapping, power plant inspection, reconnaissance, surveillance, etc (Hassanalian and Abdelkefi, 2017; Manyam et al., 2017; Stodola et al., 2018; Alvear et al., 2018; Wan et al., 2020). As a result, UAVs have received extensive attention from many scholars.

While performing military reconnaissance and rescue missions, quadrotor UAVs usually rely on accurate path planning and robust navigation and attitude controllers. However, a quadrotor UAV is an omnidirectional maneuverable aircraft with four inputs and six degrees of freedom. It is under actuated, strongly coupled, takes off and lands vertically. Therefore, it is always difficult and crucial to design an accurate and reasonable attitude controller to control and keep it stable, so as to ensure the smooth execution of missions.

Presently, a variety of trajectory tracking control methods have been extensively studied and applied by scholars. For instance, there is nonlinear proportional-integral-derivative control (Moreno-Valenzuela et al., 2018), nonlinear adaptive control technology (Avram et al., 2017), model predictive control0 (Cao et al., 2017), linear quadratic regulator control method (Faessler et al., 2017), robust linear parameter varying observer (López-Estrada et al., 2016), and sliding mode control (SMC) (Castañeda and Gordillo, 2019), and so on. Among them, SMC is more effective because of its good instantaneous performance, ease of operation, compensation for uncertain parameters, and strong anti-interference capability (Zulu and John, 2014).

In order to compensate for uncertain parameters in the design of a controller, an adaptive SMC method was proposed for the control of stability of UAVs (Mofid and Mobayen, 2018). Fuzzy logic was employed to determine the parameters needed for the adaptive sliding mode surface of the attitude control of a quadrotor UAV (Yang and Yan, 2016). A second-order SMC (2-SMC) was proposed to track the position and attitude of quadrotor UAVs (Zheng et al., 2014). A quadrotor dynamic model was divided into fully-actuated and under-actuated subsystems, a rapid terminal SMC method was then proposed for attitude control (Xiong and Zhang, 2016). A robust nonlinear control strategy was proposed by combining back-stepping with a rapid terminal SMC to track the trajectory of quadrotor UAVs (Labbadi and Cherkaoui, 2019).

In order to suppress chattering, a method was put forward by combining the integral method with SMC (Jia, 2017). This technique could effectively prevent the chattering phenomenon caused by conventional control methods. Neural network and SMC were combined to control quadrotor (Razmi, 2018). However, the vibration of the designed controller was relatively large, which caused a large maximum overshoot in the entire tracking process. Based on this, a neural network-based adaptive SMC was proposed for attitude control of quadrotor UAVs, but chattering still occurred in some cases (Razmi and Afshinfar, 2019).

With all these methods, we can effectively track the desired trajectory of a UAV and suppress the chattering phenomenon. However, the following shortcomings still exist in their practical application.

• Most scholars assume that the desired roll and pitch angles are both 0, causing over-compensation for uncertain parameters and then chattering in the design of a controller.

• During the continuous switching of a control signal, the high frequency chattering of a controller results from the fixity of parameters.

• Maximum overshoot is relatively large during chattering.

As a multi-layer forward neural network algorithm, a back propagation (BP) network can have its weight adjusted by virtue of back propagation for the arbitrary nonlinear mapping from input to output (Wu et al., 2016). In order to resolve the above problem and expand the application of neural networks, SMC and BP networks are integrated into an improved BP network based on a sliding mode tracking control for quadrotor UAVs in this paper.

The specific arrangement of the subsequent sections is as follows. The second section gives the nonlinear dynamic equations of quadrotor UAVs according to Newton-Euler equations. In the third section, a controller based on SMC is designed. In the fourth section, the parameters of a quasi-fully actuated controller are solved with an improved BP network. The fifth section presents the simulation and comparison results. Finally, conclusions are drawn in the sixth section.

2. QUADROTOR DYNAMICAL MODEL

A quadrotor is a highly coupled under- actuated system with four motors (Fig. 1). The rotation speed of four motors are controlled to generate lift and torque, which results in such movements of UAVs as lifting, movement forward, backward, left and right, pitching, rolling, yawing, and so on (Zheng et al., 2014; Xiong and Zhang, 2016; Labbadi and Cherkaoui, 2019).

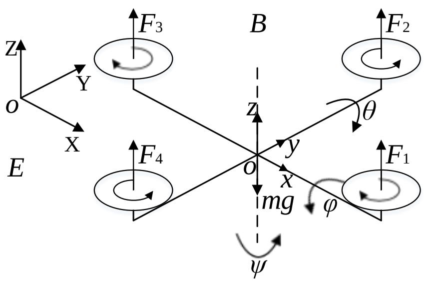

Fig. 1. Schematic of Quadrotor UAV.

Several assumptions are made to help construct a quadrotor UAV's dynamical model as follows.

Assumption 1. The quadrotor UAV has a rigid symmetrical structure;

Assumption 2. The quadrotor UAV's center of mass coincides with the origin of its body's coordinates.

In Fig. 1, F_1, F_2, F_3, F_4 denote the lift force generated by four motors, respectively. With the parameters of the UAV, four control inputs can be calculated by:

$$\begin{bmatrix} u_1 \\ u_2 \\ u_3 \\ u_4 \end{bmatrix} = \begin{bmatrix} 1 & 1 & 1 & 1 \\ l & 0 & -l & 0 \\ 0 & l & 0 & -l \\ -k & k & -k & k \end{bmatrix} \begin{bmatrix} F_1 \\ F_2 \\ F_3 \\ F_4 \end{bmatrix} \tag{1}$$

where u_1 represents the total lift force on the body in the z-axis; u_2, u_3 and u_4 are the roll, pitch and yawing torques, respectively; l represents the distance from the center of each rotor to the center of gravity; k, measured in meters, denotes the parameters of the propeller depending on propeller size, blades, air density and other parameters (Zheng et al., 2014).

Assuming that the position of the quadrotor UAV in the earth-frame (E in Fig. 1) is $\boldsymbol{P}=[x, y, z]^T$, and the attitude in the body-frame (B in Fig. 1) is $\boldsymbol{\eta}=[\varphi, \theta, \psi]^T$, according to Newton-Euler equations, the dynamic equations of the quadrotor UAV are as follows:

$$\begin{cases} u_1 \boldsymbol{R}_B^E = m\ddot{\boldsymbol{P}} - m\boldsymbol{g}_z \\ \boldsymbol{M} = \boldsymbol{J}\ddot{\boldsymbol{\eta}} + \dot{\boldsymbol{\eta}} \times \boldsymbol{J}\dot{\boldsymbol{\eta}} \end{cases} \tag{2}$$

where $\boldsymbol{R}_B^E$ denotes the rotation matrix from the body-frame to the earth-frame; m denotes the mass of the quadrotor UAV; $\boldsymbol{g}_z = [0, 0, g]^T$; $\boldsymbol{M}$ is the torque matrix $[u_2, u_3, u_4]^T$; and $\boldsymbol{J}$ denotes the inertia matrix $diag(I_x, I_y, I_z)$. By expanding Equation (2), the nonlinear dynamic model of the quadrotor UAV can be describe by:

$$\begin{cases} \ddot{x} = \dfrac{u_1}{m}(\sin\psi\sin\varphi + \cos\psi\sin\theta\cos\varphi) \\ \ddot{y} = \dfrac{u_1}{m}(-\cos\psi\sin\varphi + \sin\psi\sin\theta\cos\varphi) \\ \ddot{z} = \dfrac{u_1}{m}\cos\theta\cos\varphi - g \\ \ddot{\varphi} = \dfrac{I_y - I_z}{I_x}\dot{\theta}\dot{\psi} + \dfrac{l}{I_x}u_2 \\ \ddot{\theta} = \dfrac{I_z - I_x}{I_y}\dot{\varphi}\dot{\psi} + \dfrac{l}{I_y}u_3 \\ \ddot{\psi} = \dfrac{I_x - I_y}{I_z}\dot{\varphi}\dot{\theta} + \dfrac{d}{I_z}u_4 \end{cases} \tag{3}$$

where d represents a dimensionless scaling coefficient; φ and θ are the roll and pitch angles in the range (-π/2, π/2), respectively; and ψ is the yaw angle in the range (-π, π).

3. DESIGN OF THE STRUCTURE OF SLIDING MODE CONTROLLER

The forced variable separation of Equation (3) can be divided into the following two matrix equations:

$$\begin{bmatrix} \ddot{z} \\ \ddot{\psi} \end{bmatrix} = \begin{bmatrix} \dfrac{\cos\theta\cos\varphi}{m} & 0 \\ 0 & \dfrac{d}{I_z} \end{bmatrix} \begin{bmatrix} u_1 \\ u_4 \end{bmatrix} + \begin{bmatrix} -g \\ \dfrac{I_x - I_y}{I_z}\dot{\varphi}\dot{\theta} \end{bmatrix} \tag{4}$$

$$\begin{bmatrix} \ddot{x} \\ \ddot{y} \\ \ddot{\varphi} \\ \ddot{\theta} \end{bmatrix} = \begin{bmatrix} A_1/m & 0 & 0 & 0 \\ A_2/m & 0 & 0 & 0 \\ 0 & 0 & l/I_x & 0 \\ 0 & 0 & 0 & l/I_y \end{bmatrix} \begin{bmatrix} u_1 \\ 0 \\ u_2 \\ u_3 \end{bmatrix} + \begin{bmatrix} 0 \\ 0 \\ (I_y - I_z)\dot{\theta}\dot{\psi}/I_x \\ (I_z - I_x)\dot{\varphi}\dot{\psi}/I_y \end{bmatrix} \tag{5}$$

where $A_1 = \cos\psi\cos\varphi\sin\theta + \sin\psi\sin\varphi$, $A_2 = -\cos\psi\sin\varphi + \sin\psi\cos\varphi\sin\theta$.

The input matrices of the above equations reveal that the quadrotor model is composed of quasi-fully actuated subsystems and quasi-under actuated subsystems. In addition, according to Equation (5), the control of the quasi-under actuated subsystems must be under the coupling control of u_2, u_3 and u_1 to change the state variable x, y, θ, φ of the UAV.

The structure of the proposed control system is illustrated in Fig. 2.

3.1. The control Strategy

The control of the quasi-fully actuated subsystem is intended to ensure that u_1 and u_4 makes the state variable height z and yaw angle ψ converge to the desired state z_d and ψ_d. The height error is taken as $e_z = z_d - z$, while the yaw error is $e_\psi = \psi_d - \psi$. Then, the switching functions of the sliding mode altitude control and yaw angle control are defined as:

$$\begin{cases} s_z = c_z e_z + \dot{e}_z \\ s_\psi = c_\psi e_\psi + \dot{e}_\psi \end{cases} \tag{6}$$

where c_z and c_ψ are the parameters to be solved in the design.

In the design of quasi-under actuated controllers, most scholars assume that the desired roll angle and pitch angle are both 0, such as (Zheng et al., 2014; Xiong and Zhang, 2016; Labbadi and Cherkaoui, 2019; Jia et al., 2017; Razmi, 2018; Razmi and Afshinfar, 2019), etc. In fact, within a defined time interval, after the desired trajectory is given

by $\ddot{x}_d$, $\ddot{y}_d$, $\ddot{z}_d$ & $\ddot{\psi}_d$, the desired roll angle and pitch angle of a quadrotor UAV are also given since it is highly coupled.

We should therefore minimize correction errors in the design of a quasi-under actuated controller since the desired roll angle and pitch angle are ignored.

Firstly, from the first three equations of Equations (3), we can obtain

$$\begin{cases} \tan\theta = \dfrac{\ddot{x}\cos\psi + \ddot{y}\sin\psi}{\ddot{z}+g} \\ \tan\varphi = \dfrac{\cos\theta(\ddot{x}\sin\psi - \ddot{y}\cos\psi)}{\ddot{z}+g} \end{cases} \tag{7}$$

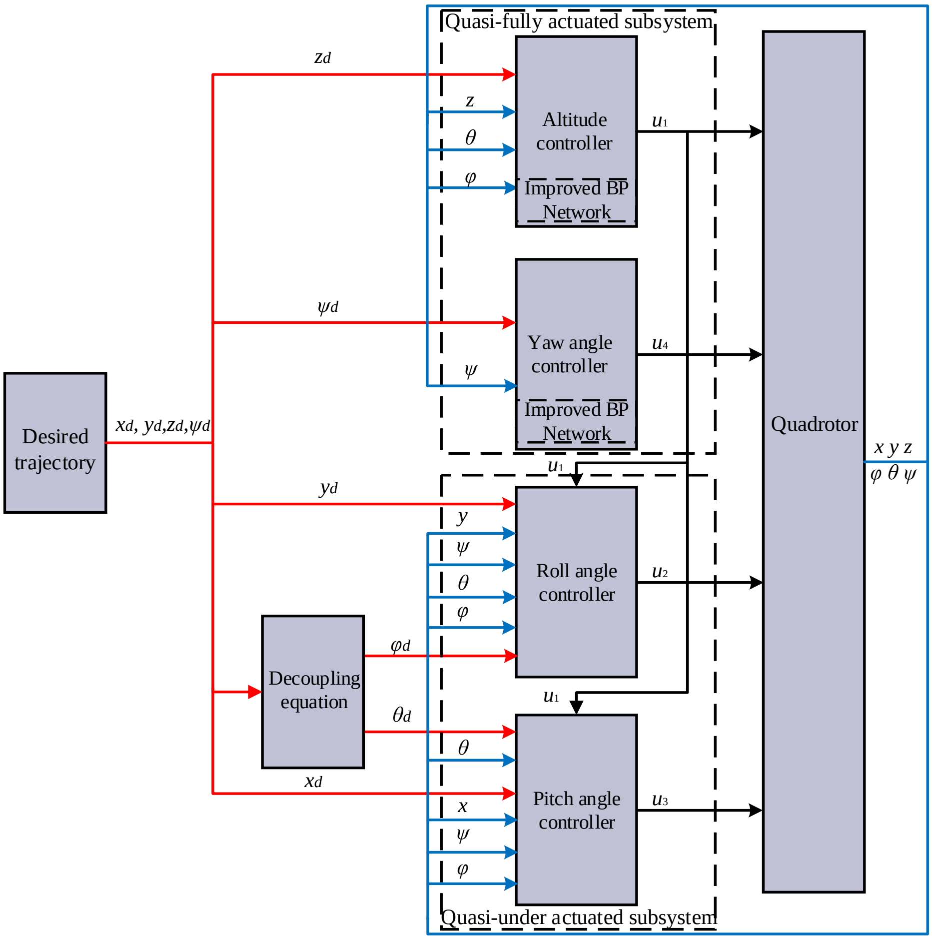

Fig. 2. The structure of the proposed control system .

Roll and pitch angles are defined within the range (−π/2, π/2). Only the quadrant within the defined range is therefore taken into account while using the arctan function. We can therefore obtain the decoupling calculation formula of desired roll angle φ_d and desired pitch angle θ_d as follows:

$$\begin{cases} \varphi_d = \arctan(\dfrac{\cos\theta_d\,(\ddot{x}_d \sin\psi_d - \ddot{y}_d \cos\psi_d)}{\ddot{z}_d + g}) \\ \theta_d = \arctan(\dfrac{\ddot{x}_d \cos\psi_d + \ddot{y}_d \sin\psi_d}{\ddot{z}_d + g}) \end{cases} \quad (8)$$

On this basis, it is intended to ensure that the coupled control of u_2 with u_3 and u_1 makes the corresponding state variables x and θ converge to the desired state x_d and θ_d, respectively. Moreover, y and φ can converge to the desired value y_d and φ_d, respectively. The corresponding errors are taken as $e_x = x_d - x$, $e_\theta = \theta_d - \theta$, $e_y = y_d - y$ and $e_\varphi = \varphi_d - \varphi$.

As a result, we define the switching functions (9) of quasi-under actuated controller, each as a sum of position and velocity tracking errors at relevant coordinates (Ashrafiuon and Erwin, 2008), that is:

$$\begin{cases} s_\varphi = c_1 e_y + c_2 \dot{e}_y + c_3 e_\varphi + c_4 \dot{e}_\varphi \\ s_\theta = c_5 e_x + c_6 \dot{e}_x + c_7 e_\theta + c_8 \dot{e}_\theta \end{cases} \quad (9)$$

Where $c_i (i = 1, \cdots, 8)$ are the switching functions coefficients, which are real positive coefficients.

3.2. Solving the control law

Therefore, the sliding mode switching function differential equations designed for the whole UAV system are:

$$\begin{cases} \dot{s}_z = c_z \dot{e}_z + \ddot{e}_z \\ \dot{s}_\psi = c_\psi \dot{e}_\psi + \ddot{e}_\psi \\ \dot{s}_\varphi = c_1 \dot{e}_y + c_2 \ddot{e}_y + c_3 \dot{e}_\varphi + c_4 \ddot{e}_\varphi \\ \dot{s}_\theta = c_5 \dot{e}_x + c_6 \ddot{e}_x + c_7 \dot{e}_\theta + c_8 \ddot{e}_\theta \end{cases} \quad (10)$$

The quadrotor is a rigid and symmetrical body, then $I_x = I_y$, so that Equation (3) can be substituted into Equation (10) to obtain:

$$\begin{cases} \dot{s}_z = c_z \dot{e}_z + \ddot{z}_d - \dfrac{u_1}{m}\cos\theta\cos\varphi + g \\ \dot{s}_\psi = c_\psi \dot{e}_\psi + \ddot{\psi}_d - \dfrac{d}{I_z} u_4 \\ \dot{s}_\varphi = c_1 \dot{e}_y + c_2 \ddot{e}_y + c_3 \dot{e}_\varphi \\ \qquad + c_4 \left(\ddot{\varphi}_d - \dfrac{I_y - I_z}{I_x} \dot{\theta}\dot{\psi} - \dfrac{l}{I_x} u_2 \right) \\ \dot{s}_\theta = c_5 \dot{e}_x + c_6 \ddot{e}_x + c_7 \dot{e}_\theta \\ \qquad + c_8 \left(\ddot{\theta}_d - \dfrac{I_z - I_x}{I_y} \dot{\varphi}\dot{\psi} - \dfrac{l}{I_y} u_3 \right) \end{cases} \quad (11)$$

To obtain the control laws for maintaining the system in sliding mode the derivative of the switching functions devised as the following:

$$\dot{s}_i = -\varepsilon_i \tanh(s_i) - \beta_i s_i \quad (12)$$

where $i = z, \psi, \varphi, \theta$, ε_i and β_i is the positive coefficients.

Substituting Equation (3) and Equation (12) into Equation (11), and solving the result with respect to the control law u_1 of altitude controller, control law u_2 of yaw angle controller, control law u_3 of roll angle controller and control law u_4 of pitch angle controller, the four control laws (13) are obtained:

$$\begin{cases} u_1 = \dfrac{m(c_z \dot{e}_z + \ddot{z}_d + g + \varepsilon_z \tanh(s_z) + \beta_z s_z)}{\cos\theta\cos\varphi} \\ u_2 = \dfrac{I_x}{l c_4} (c_2 \ddot{y}_d + c_1 \dot{e}_y + c_3 \dot{e}_\varphi + \ddot{\varphi}_d + \beta_\varphi s_\varphi \\ \qquad - c_2 \dfrac{u_1(\sin\psi\sin\theta\cos\varphi - \cos\psi\sin\varphi)}{m} \\ \qquad - \dfrac{1}{I_x}(I_y - I_z)\dot{\theta}\dot{\varphi} + \varepsilon_\varphi \tanh(s_\varphi)) \\ u_3 = \dfrac{I_y}{l c_8} (c_5 \dot{e}_x + c_6 \ddot{x}_d + c_7 \dot{e}_\theta + \ddot{\theta}_d + \beta_\theta s_\theta \\ \qquad + c_6 \dfrac{u_1(\sin\psi\sin\varphi + \cos\psi\sin\theta\cos\varphi)}{m} \\ \qquad - \dfrac{1}{I_y}(I_z - I_x)\dot{\varphi}\dot{\psi} + \varepsilon_\theta \tanh(s_\theta)) \\ u_4 = \dfrac{I_z}{d}(c_\psi \dot{e}_\psi + \ddot{\psi}_d + \varepsilon_\psi \tanh(s_\psi) + \beta_\psi s_\psi) \end{cases} \quad (13)$$

3.3. Stability analysis

Proposition. *The nonlinear control system of the quadrotor* (4) & (5), *that uses the switching functions* (6) & (9), *and the control laws* (13), *is asymptotically stable*.

Proof. The positive Lyapunov function candidate is selected as:

$$V = \sum_{k=i}^{i=z,\psi,\varphi,\theta} s_k^2 / 2 \quad (14)$$

With the consideration of Equation (12), the derivatives of V is:

$$\begin{aligned} \dot{V} &= \sum_{k=i}^{i=z,\psi,\varphi,\theta} s_k(-\varepsilon_k \tanh(s_k) - \beta_k s_k) \\ &\le \sum_{k=i}^{i=z,\psi,\varphi,\theta} (-\varepsilon_k \mid s_k \mid - \beta_k {s_k}^2) \le 0 \end{aligned} \quad (15)$$

From Equation (15), $\dot{V}$ will always be negative, according to the Lyapunov stability theorem, the nonlinear dynamic model of the quadrotor is asymptotically stable under the designed control law. Therefore, the proposition has been verified.

So far, the parameters to be solved are c_z, c_ψ, ε_z and ε_ψ. As for other parameters, the values in Zheng et al., 2014 were adopted.

4. IMPROVED BP NETWORK

Since the parameters c_z, c_ψ, ε_z and ε_ψ of the altitude controller and the yaw angle controller are still unknown, most scholars take the above parameters to a constant value, but with the reduction of the error, if the parameters cannot be adjusted in time, it will cause chattering phenomenon.

A BP network is a forward neural network algorithm. It can have its weights adjusted by virtue of BP, and is featured by good fault tolerance (Gonzalez-Garcia et al., 2020). As shown in Fig. 2, it is envisaged that the BP network can be improved to suppress controller chattering phenomenon while solving the parameters of a quasi-fully actuated switching function (6).

4.1. Standard BP network

Taking the altitude controller as an example, the block schema in Fig. 3, is associated with Equation (12). Here $e_z = z_d - z$. It is observed that the structure is similar to a BP network, but a correction term $-\beta_z s_z$ is added to eliminate the distortion of $\tanh(s_z)$. The parameters to be solved are c_z, ε_z.

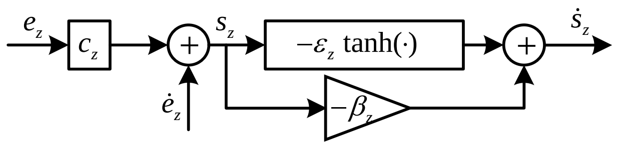

Fig. 3. The structure of the reaching law.

To track the desired altitude, as accurately as possible, and conveniently calculate the parameters of the switching function s_z with BP network, we consider the performance error E_z (16):

$$E_z = e_z^{\,2}/2 = (z_d - z)^2/2 \tag{16}$$

With the steepest gradient descent method, we can get:

$$\begin{cases} \varepsilon_{z,k+1} = \varepsilon_{z,k} - \alpha_z \partial E_{z,k} / \partial \varepsilon_{z,k} \\ c_{z,k+1} = c_{z,k} - \alpha_z \partial E_{z,k} / \partial c_{z,k} \end{cases}, \ k = 1, 2, \cdots, n \tag{17}$$

Where, k represents the index of time series, which is the time $k\delta$, δ is the constant sampling time, consistent with the fixed step size of the continuous system solver. The α_z is the learning rate. Let $\partial E_{z,k} / \partial \varepsilon_{z,k}$ and $\partial E_{z,k} / \partial c_{z,k}$ are the gradient vector of the output error to ε_z and c_z, respectively, when the neural network iterates for the k^{th} time. Then, according to the chain derivation rule, we obtain:

$$\frac{\partial E_{z,k}}{\partial \varepsilon_{z,k}} = \frac{\partial E_{z,k}}{\partial z_k}\frac{\partial z_k}{\partial u_{1,k}}\frac{\partial u_{1,k}}{\partial \varepsilon_{z,k}} = -\frac{m e_{z,k} \tanh(s_{z,k})}{\cos\theta \cos\varphi}\frac{\partial z_k}{\partial u_{1,k}} \tag{18}$$

$$\begin{aligned} \frac{\partial E_{z,k}}{\partial c_{z,k}} &= \frac{\partial E_{z,k}}{\partial z_k}\frac{\partial z_k}{\partial u_{1,k}}\frac{\partial u_{1,k}}{\partial s_{z,k}}\frac{\partial s_{z,k}}{\partial c_{z,k}} \\ &= -\frac{m(e_{z,k})^2}{\cos\theta\cos\varphi}\left[\frac{\varepsilon_{z,k}\, 4(e_{z,k})^{-2s_{z,k}}}{(1+e^{-2s_{z,k}})^2} + \beta_z\right]\frac{\partial z_k}{\partial u_{1,k}} \end{aligned} \tag{19}$$

where $\partial z_k / \partial u_{1,k}$ is unknown. But, partial derivatives are crude replacement by their signs (Saerens and Soquet, 1991). So we assume that $sign(\nabla z_k / \nabla u_{1,k})$ is approximately $\partial z_k / \partial u_{1,k}$.

Substituting Equations (18) and (19) into Equation (17), the correction equations of $\varepsilon_{z,k}$ and $c_{z,k}$ under the standard BP network are:

$$\begin{aligned} \varepsilon_{z,k+1} &= \varepsilon_{z,k} - \alpha_z \frac{\partial E_{z,k}}{\partial \varepsilon_{z,k}} \\ &= \varepsilon_{z,k} + \frac{\alpha_z m e_{z,k} \tanh(s_{z,k})}{\cos\theta\cos\phi} sign\left(\frac{\nabla z_k}{\nabla u_{1,k}}\right) \end{aligned} \tag{20}$$

$$\begin{aligned} c_{z,k+1} &= c_{z,k} - \alpha_z \frac{\partial E_{z,k}}{\partial c_{z,k}} \\ &= c_{z,k} + \frac{m\alpha_z (e_{z,k})^2}{\cos\theta\cos\phi} sign\left(\frac{\nabla z_k}{\nabla u_{1,k}}\right)\left[\frac{\varepsilon_{z.k}\, 4(e_{z,k})^{-2s_{z,k}}}{(1+(e_{z,k})^{-2s_{z,k}})^2} + \beta_z\right] \end{aligned} \tag{21}$$

4.2. BP network with variable learning rate momentum

When the selected learning rate is large, the controller gets closer and closer to the desired state in the tracking process, which will cause a large overshoot at each step. When the selected learning rate is small, a small amount of momentum energy will be accumulated and the system will fall into local optimum. In this case, it cannot jump out of the local optimum in time.

For better stability and lower oscillation, it is necessary to make the learning rate dynamically adjust to the variation of error. Therefore, a variable learning rate factor (k_{inc} & k_{dec}) is introduced for this purpose. When the error tends to 0 in a decreasing way, the correction is performed correctly, so that the step size can be increased. At this time, the learning rate $\alpha_{z,k}$ is multiplied by the incremental factor $k_{inc}(1 < k_{inc})$. When the error becomes larger and larger, correction is performed excessively, so that the step size should be reduced. In this case, the learning rate $\alpha_{z,k}$ is multiplied by the decrement factor $k_{dec}(0 < k_{dec} < 1)$. Through the above operations, the updated learning rate $\alpha_{z,k+1}$ can be obtained.

While changing the learning rate, a large learning rate may easily cause the learning process to diverge, and a small learning rate will lower the calculation efficiency. Considering the fastest gradient descent algorithm and the variable learning rate, a momentum factor $\eta(0 < \eta < 1)$ is therefore introduced to ensure both convergence and computational efficiency. Eventually, we can talk about a dynamic operator Δ :

$$\Delta\varepsilon_{z,k+1} = \eta\Delta\varepsilon_{z,k} + \alpha_{z,k}(1-\eta)\frac{\partial E_{z,k}}{\partial \varepsilon_{z,k}} \tag{22}$$

$$\Delta c_{z,k+1} = \eta\Delta c_{z,k} + \alpha_{z,k}(1-\eta)\frac{\partial E_{z,k}}{\partial c_{z,k}} \tag{23}$$

This operator is intended to adjust the current correction using the result of the previous correction. When the previous correction is excessive, the two terms of the adjustment operator will have opposite signs $(\eta \geq 1, E_{z,k-1} \geq E_z)$. The current correction will therefore be reduced to achieve oscillation suppression. When the previous correction is insufficient, the two terms of the adjustment operator will have identical signs $(0 < \eta < 1, E_{z,k} > E_{z,k-1})$. The current correction will be then increased to accelerate the correction. Adding this momentum factor will not cause the learning process to diverge, since the operator will be corrected in time if the correction is excessive or insufficient. In this case, correction heads towards convergence.

After sorting out the above content, the correction equations of $\varepsilon_{z,k}$ and $c_{z,k}$ in the improved BP network can be obtained as:

$$\varepsilon_{z,k+1} = \varepsilon_{z,k} + \Delta\varepsilon_{z,k+1} = \varepsilon_{z,k} + \eta\Delta\varepsilon_{z,k} + \alpha_{z,k}(1-\eta)\frac{\partial E_{z,k}}{\partial \varepsilon_{z,k}} \tag{24}$$

$$c_{z,k+1} = c_{z,k} + \Delta c_{z,k+1} = c_{z,k} + \eta\Delta c_{z,k} + \alpha_{z,k}(1-\eta)\frac{\partial E_{z,k}}{\partial c_{z,k}} \tag{25}$$

Similarly, when a neural network iterates for the k^{th} time, the gradient vector of output error to ε_ψ and c_ψ is

$$\begin{aligned}\frac{\partial E_{\psi,k}}{\partial \varepsilon_{\psi,k}} &= \frac{\partial E_{\psi,k}}{\partial \psi_k}\frac{\partial \psi_k}{\partial u_{4,k}}\frac{\partial u_{4,k}}{\partial \varepsilon_{\psi,k}} \\ &= -\frac{e_{\psi,k} I_z \tanh(s_{\psi,k})}{d} sign\left(\frac{\nabla \psi_k}{\nabla u_{4,k}}\right)\end{aligned} \tag{26}$$

$$\begin{aligned}\frac{\partial E_{\psi,k}}{\partial c_{\psi,k}} &= \frac{\partial E_{\psi,k}}{\partial \psi_k}\frac{\partial \psi_k}{\partial u_{4,k}}\frac{\partial u_{4,k}}{\partial s_{\psi,k}}\frac{\partial s_{\psi,k}}{\partial c_{\psi,k}} \\ &= -(e_{\psi,k})^2\frac{I_z}{d}\left[\frac{\varepsilon_{\psi,k} 4(e_{\psi,k})^{-2s_{\psi,k}}}{(1+(e_{\psi,k})^{-2s_{\psi,k}})^2} + \beta_\psi\right] sign\left(\frac{\nabla \psi_k}{\nabla u_{4,k}}\right)\end{aligned} \tag{27}$$

Therefore, the correction equations of $\varepsilon_{\psi,k}$ and $c_{\psi,k}$ in the standard BP network are:

$$\begin{aligned}\varepsilon_{\psi,k+1} &= \varepsilon_{\psi,k} - \alpha_\psi \frac{\partial E_{\psi,k}}{\partial \varepsilon_{\psi,k}} \\ &= \varepsilon_{\psi,k} + \frac{\alpha_\psi I_z e_{\psi,k}}{d}\tanh(s_{\psi,k}) sign\left(\frac{\nabla \psi_k}{\nabla u_{4,k}}\right)\end{aligned} \tag{28}$$

$$\begin{aligned}c_{\psi,k+1} &= c_{\psi,k} - \alpha_\psi \frac{\partial E_{\psi,k}}{\partial c_{\psi,k}} \\ &= c_{\psi,k} + \frac{\alpha_\psi I_z (e_{\psi,k})^2}{d} sign\left(\frac{\nabla \psi_k}{\nabla u_{4,k}}\right) \\ &\left[\frac{\varepsilon_{\psi,k} 4(e_{\psi,k})^{-2s_{\psi,k}}}{(1+(e_{\psi,k})^{-2s_{\psi,k}})^2} + \beta_\psi\right]\end{aligned} \tag{29}$$

The correction equations of $\varepsilon_{\psi,k}$ and $c_{\psi,k}$ in the improved BP network are:

$$\begin{aligned}\varepsilon_{\psi,k+1} &= \varepsilon_{\psi,k} + \Delta\varepsilon_{\psi,k+1} \\ &= \varepsilon_{\psi,k} + \eta\Delta\varepsilon_{\psi,k} + \alpha_{\psi,k}(1-\eta)\frac{\partial E_{\psi,k}}{\partial \varepsilon_{\psi,k}}\end{aligned} \tag{30}$$

$$\begin{aligned}c_{\psi,k+1} &= c_{\psi,k} + \Delta c_{\psi,k+1} \\ &= c_{\psi,k} + \Delta\eta c_{\psi,k} + \alpha_{\psi,k}(1-\eta)\frac{\partial E_{\psi,k}}{\partial c_{\psi,k}}\end{aligned} \tag{31}$$

5. SIMULATION, RESULTS AND DISCUSSIONS

This section presents a simulation of the proposed method using MATLAB/Simulink R2020b (64 bit) software. The software was installed in a workstation with an AMD Ryzen 9 3900XT 12-Core Processor, 32GB, 64-bit Win10 operating system.

In the model of this paper, since the IBP module operates in discrete time and the other operates in continuous time, in order to facilitate the solution, a continuous solver with a fixed step size δ is used to solve the problem. The step δ is regarded as the sampling time of IBP module.

Under ideal conditions, this paper uses 2-SMC (Zheng et al., 2014), standard BP network under SMC and the proposed method to control the UAV to track the desired trajectory, and then verify the effectiveness of the proposed method.

The parameters of the quadrotor UAV used in the simulation are shown in Table 1.

Table 1. Quadrotor parameters.

Parameter	Value
m(kg)	1.1
l(m)	0.21
I_x(N·s^2·rad^{-1})	1.22
I_y(N·s^2·rad^{-1})	1.22
I_z(N·s^2·rad^{-1})	2.2
g(m·s^{-2})	9.8
k(N ms^{-2})	2
d	1

Moreover, the proposed controller parameters are given in Table 2. In this table, $c_i, (i = 1, 2, \cdots, 8)$, ε_θ and ε_φ is taken directly from Zheng et al., 2014.

The starting position of the quadrotor UAV is (0,0,0) m. The initial Euler angle is (0,0,0) rad. The desired 3D tracking trajectory is shown in Table 3:

Table 2. Controller parameters.

Parameter	Value	Parameter	Value
$\alpha_{z,0}$	0.01	$\alpha_{\psi,0}$	0.1
$c_{z,0}$	0.1	$c_{\psi,0}$	0.1
$\varepsilon_{z,0}$	0.1	$\varepsilon_{\psi,0}$	0.1
ε_θ	0.5	ε_φ	0.5
β_z	0.3	β_ψ	2
β_θ	5	β_φ	5
k_{inc}	1.1	k_{dec}	0.9
c_3, c_7	6	η	1.5 or 0.5
c_4, c_8	1	δ	1.8 s
c_1		$-6m/(u_1 \cos\psi)$	
c_2		$-11m/(u_1 \cos\psi)$	
c_5		$6m/(u_1 \cos\psi \cos\varphi)$	
c_6		$11m/(u_1 \cos\psi \cos\varphi)$	

Table 3. The desired 3D tracking trajectory.

Times / s	Values / m	Values / rad
0~10	[0.6, 0.6, 0.6]	0.5
10~20	[0.3, 0.6, 0.6]	
20~30	[0.3, 0.3, 0.6]	
30~40	[0.6, 0.3, 0.6]	
40~50	[0.6, 0.6, 0.6]	
50~60	[0.6, 0.6, 0]	
60~90	[0.6, 0.6, 0]	0

In order to demonstrate its effectiveness, the proposed method is compared with the standard BP network under SMC and 2-SMC, respectively.

Figure 4 gives the simulation results of the quadrotor UAV tracking the desired trajectory under the drive of these three methods.

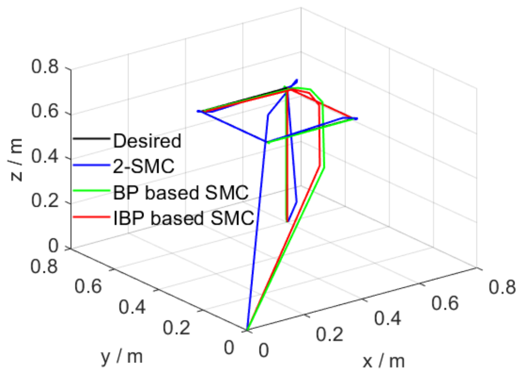

Fig. 4. The quadrotor's path.

The simulation results of the quadrotor UAV tracking the reference position x_d, y_d and z_d under the drive of these three methods, respectively, are shown in Fig. 5. As revealed in the figure, after the system reaches a steady state, the chattering phenomenon and the maximum overshoot are greatly reduced by the proposed method when compared with the other two methods when a reference position is tracked. The tracking accuracy of the proposed method is higher than that of the standard BP network under SMC.

Figure 6 shows the simulation results of the quadrotor UAV tracking the reference attitude φ_d, θ_d and ψ_d under the drive of these three methods, respectively. Obviously, the actual pitch and roll angles under the drive of the proposed method are greater than that under the drive of the other two methods when the quadrotor UAV tracks the desired pitch and roll angles.

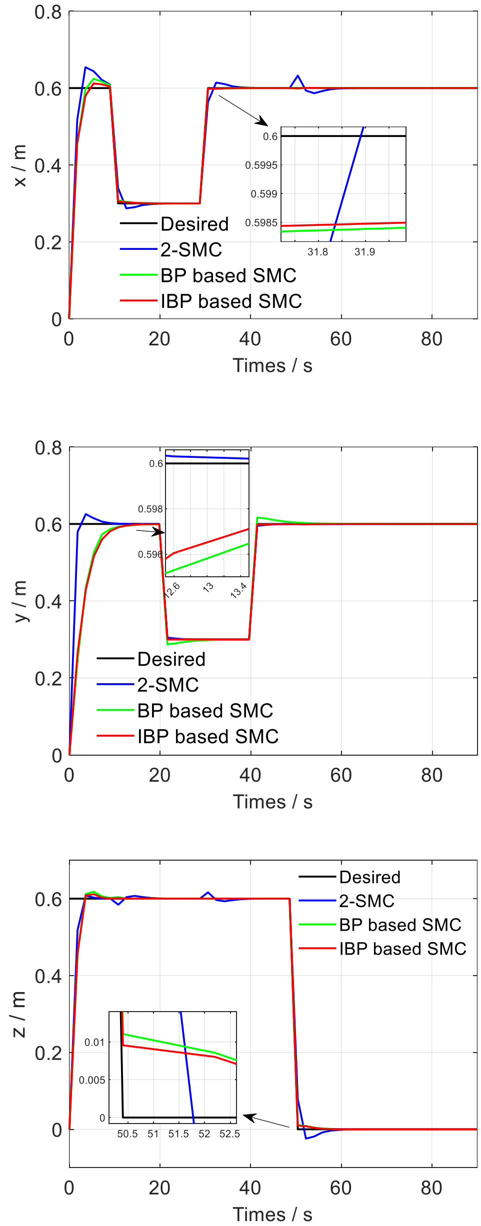

Fig. 5. Position tracking results (x, y, z).

In this paper, the desired pitch and roll angles are first determined by virtue of decoupling according to the desired trajectory, and then tracked in the design controller. The other two methods are devised by assuming that the desired pitch and roll angles are zero. Therefore, the angles obtained by the proposed method are naturally larger even with the same compensation for uncertain parameters. The comparison chart of errors is analyzed. It is found that the angle compensation required under the proposed method is much smaller than that required by the other two methods. Moreover, after the system reaches a steady state, the chattering phenomenon is significantly reduced. Evidently, in the drive of the proposed method, only a small correction is needed to make the quadrotor UAV accurately track the desired attitude, so as to enhance the stability of attitude tracking.

Four control inputs vary over time under the drive of these three methods as revealed in Fig. 7. It is obvious that these control inputs have fewer chattering phenomena under the proposed method than the other two methods, after the system reaches a steady state. Moreover, the maximum overshoot under the proposed method is significantly smaller when chattering occurs, which ensures the stability of control inputs.

Figure 8 presents the variation switching function over time under the drive of these three methods. It is revealed that the designed switching function gradually attenuates and approaches the equilibrium point 0. However, the switching function designed under the proposed method has a good suppression of chattering and a small maximum overshoot compared with the other two methods.

The parameter variation of the designed quasi-fully actuated controllers u_1 and u_4 over time is presented in Figs. 9 and 10, respectively. It is found that the parameters can be adjusted dynamically under the drive of the proposed method. For this reason, a better tracking effect is achieved by the proposed method than the other two methods.

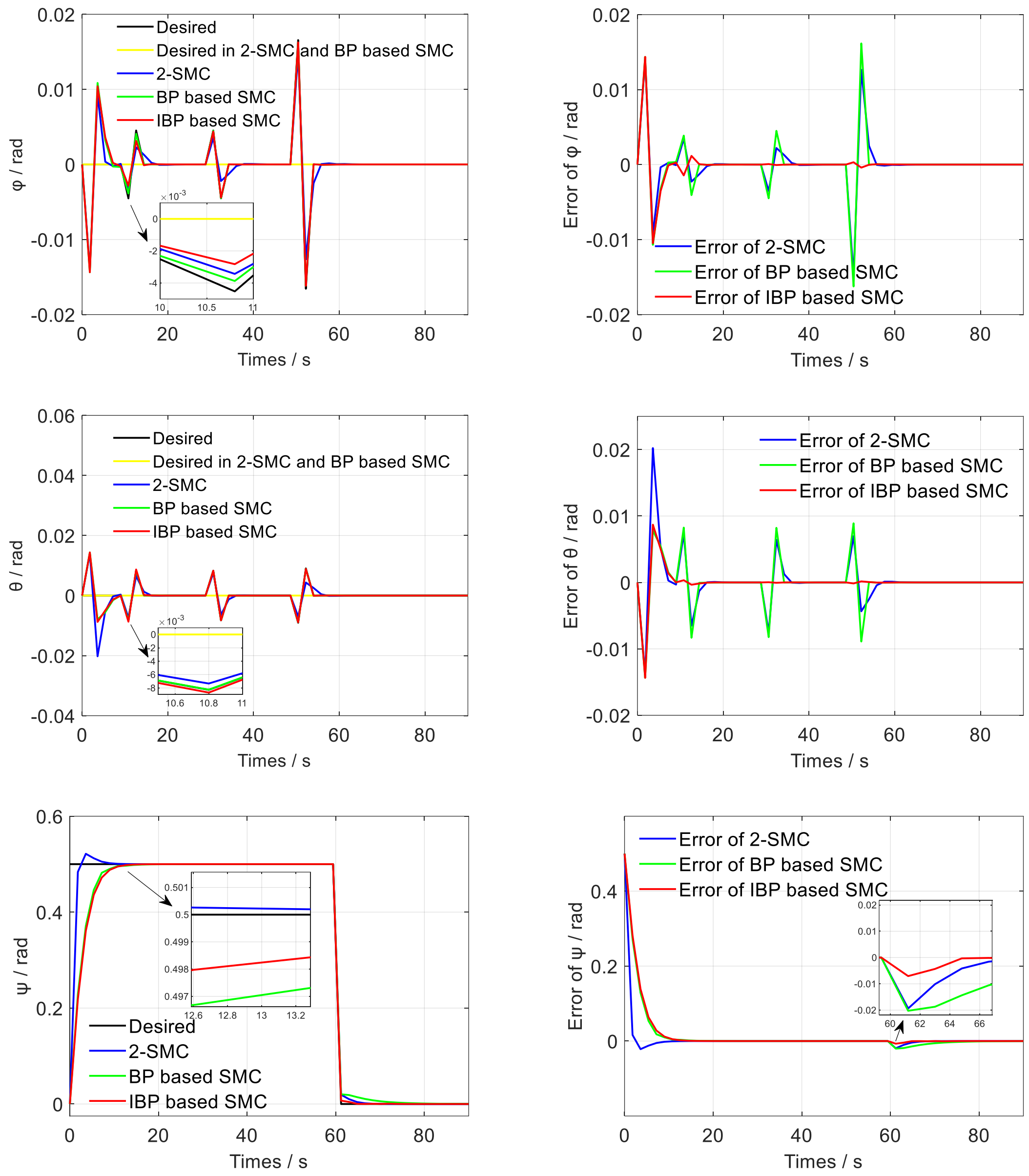

Fig. 6. Attitude tracking results and error results (φ, θ, ψ).

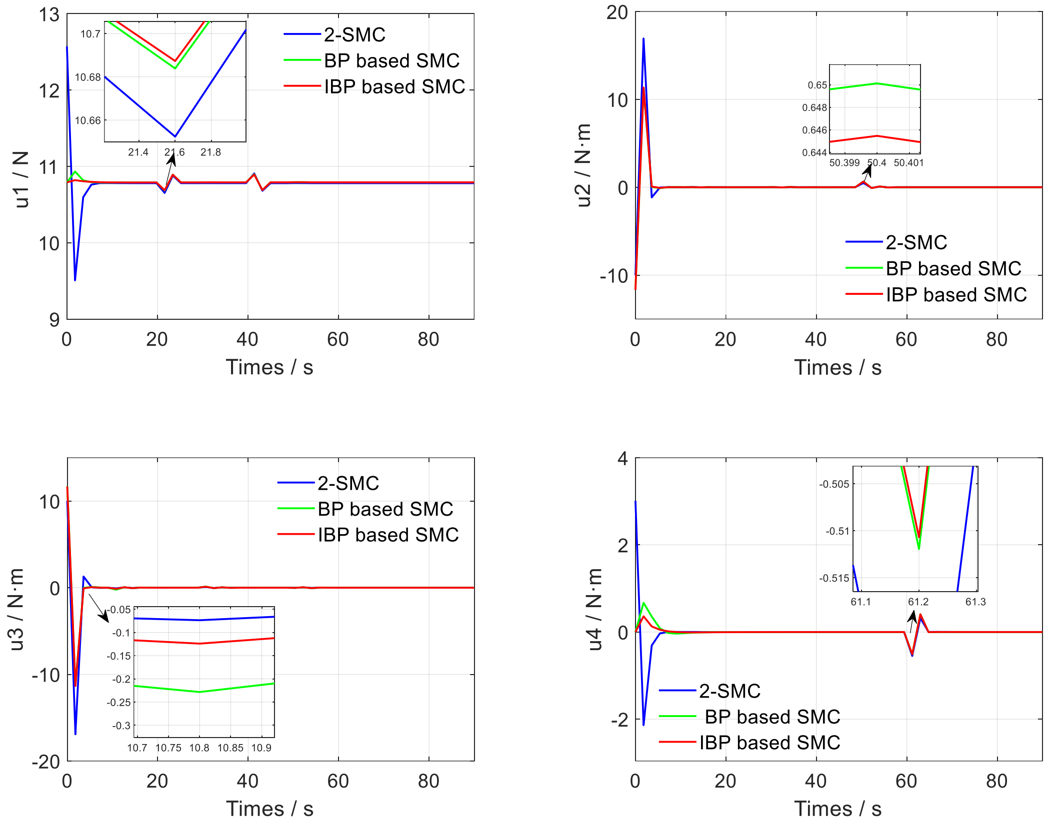

Fig. 7. Control inputs (u_1, u_2, u_3, u_4).

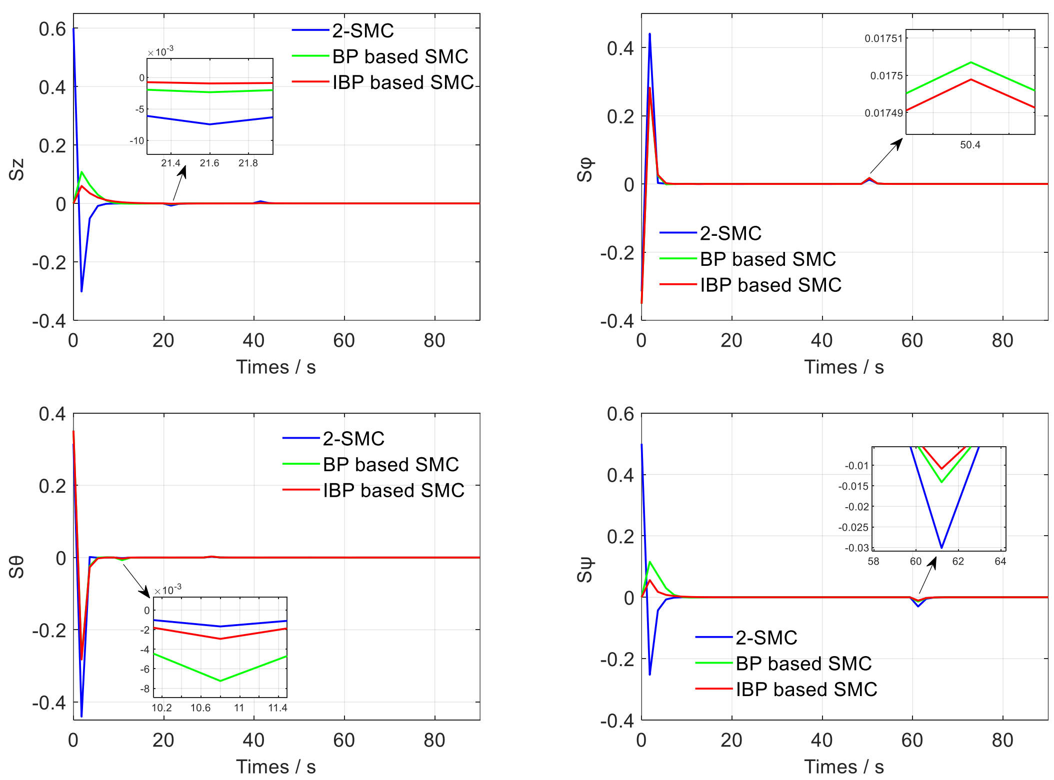

Fig. 8. The switching function ($s_z, s_\varphi, s_\theta, s_\psi$).

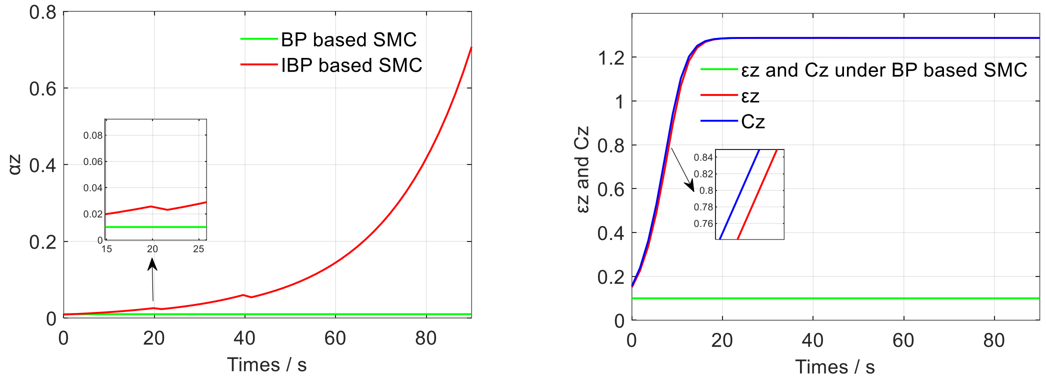

Fig. 9. Adjustable parameters for controller u_1.

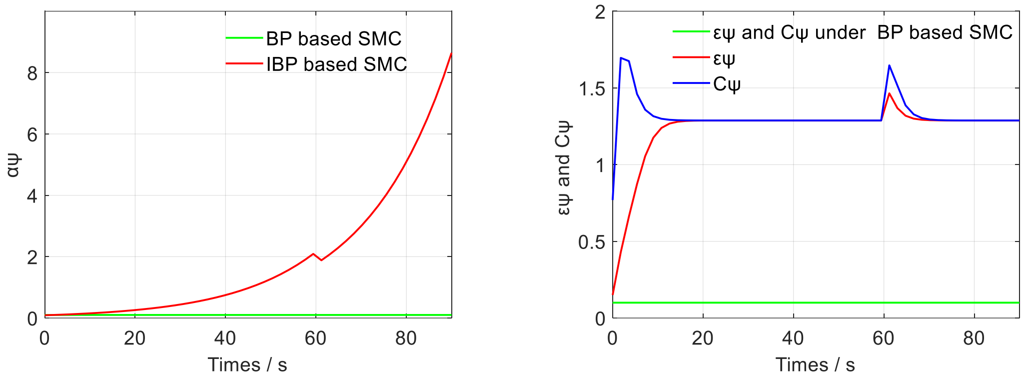

Fig. 10. Adjustable parameters for controller u_4.

In brief, the proposed method can effectively track the desired position and attitude. Compared with 2-SMC and standard BP network under SMC, after the system reaches a steady state, it can efficiently suppress the chattering phenomenon during the entire tracking process. Moreover, it can greatly reduce the maximum overshoot when chattering occurs, so as to make the controllers more stable and reliable.

6. CONCLUSION

In this paper, an improved BP network-based sliding model tracking control is studied to realize the accurate tracking of a quadrotor UAV position and attitude. In order to prevent the overcompensation of parameters, the inverse solution of the expected state is given first. In order to suppress the chattering phenomenon, on the basis of the standard BP network, variable learning rate and momentum factor are introduced. Furthermore, the effect of tracking the desired trajectory of the proposed method is compared with that of 2-SMC and the standard BP network under SMC. Simulation results verify that the proposed method has the advantages of smaller overshoot, less chatter when reaching steady state, and high precision. It can quickly recover to stable state even in the case of continuous switching of control signals. It has good adaptability and versatility, and effectively expands the application range of neural network algorithm.

ACKNOWLEDGEMENT

This work was partially supported by the National Natural Science Foundation of China (Grant No. 62073334).

DATA AVAILABILITY

The data that support the findings of this study are included within the article.

CONFLICTS OF INTEREST

The authors declare that they have no conflicts of interest.

REFERENCES

Alvear O, Calafate CT, Zema NR, Natalizio E , Hernández-Orallo E , Cano J-C and Manzoni P . (2018).A discretized approach to air pollution monitoring using UAV-based sensing. *Mobile Networks and Applications*, *23*(6): 1693–1702.

Ashrafiuon H and Erwin RS. (2008). Sliding mode control of underactuated multibody systems and its application to shape change control. *International Journal of Control*, *81*(12): 1849–58.

Avram. R.C., Zhang X. and Muse. J.. (2017). Quadrotor Actuator Fault Diagnosis and Accommodation Using Nonlinear Adaptive Estimators. *IEEE Trans. Control Systems Technology*, *25*(6): 2219–2226.

Cao G., Lai E.M.-K. and Alam F.. (2017). Gaussian Process Model Predictive Control of an Unmanned Quadrotor. *Journal of Intelligent & Robotic Systems*, *88*: 147–162.

Castañeda H. and Gordillo J.L.. (2019). Spatial Modeling and Robust Flight Control Based on Adaptive Sliding Mode Approach for a Quadrotor MAV. *Journal of Intelligent & Robotic Systems*, *93*: 101–111.

Faessler M., Falanga D. and Scaramuzza D.. (2017). Thrust

Mixing, Saturation, and Body-Rate Control for Accurate Aggressive Quadrotor Flight. *IEEE Robotics Automation Letters*, *2*(2): 476–482.

Gonzalez-Garcia A, Barragan-Alcantar D, Collado-Gonzalez I and Garrido L. (2020). Control of an Unmanned Surface Vehicle based on adaptive dynamic programming and deep reinforcement learning. *Pro of the international conference on deep learning technologies*, 118–122.

Hassanalian. M. and Abdelkefi. A.. (2017). Classifications, applications, and design challenges of drones: a review. *Prog. Aerosp*, *91*, 99–131.

Jia Z., Yu J., Mei Y., Chen Y, Shen Y and Ai X. (2017). Integral backstepping sliding mode control for quadrotor helicopter under external uncertain disturbances. *Aerospace Science and Technology*, *68*: 299–307.

Labbadi M. and Cherkaoui M.. (2019). Robust adaptive backstepping fast terminal sliding model controller for uncertain quadrotor UAV. *Aerospace Science and Technology*, *93*: 1–14.

López-Estrada F.R., Ponsart J.C., Theilliol D., Zhang Y.M and Astorga-Zaragoza C-M. (2016). LPV Model-Based Tracking Control and Robust Sensor Fault Diagnosis for a Quadrotor UAV. *Journal of Intelligent & Robotic Systems*, *84*: 163–177.

Manyam. S.G., Rasmussen. S., Casbeer. D.W., Kalyanam. K. and Manickam. S.. (2017). Multi-UAV routing for persistent intelligence surveillance and reconnaissance missions. *Proc. of International Conference on Unmanned Aircraft Systems*, 573–580.

Mofid O. and Mobayen S.. (2018). Adaptive sliding mode control for finite-time stability of quad-rotor UAVs with parametric uncertainties. *ISA Transactions*, *72*: 1–14.

Moreno-Valenzuela. J., Pérez-Alcocer. R., Guerrero-Medina. M. and Dzul. A. . (2018). Nonlinear PID-Type Controller for Quadrotor Trajectory Tracking. *IEEE/ASME Trans on Mechatron*, *23*(5): 2436–2447.

Razmi H. (2018). Adaptive neural network based sliding mode altitude control for a quadrotor UAV. *Journal of Central South University*, *25*(11): 2654–2663.

Razmi H and Afshinfar S . (2019). Neural network-based adaptive sliding mode control design for position and attitude control of a quadrotor UAV. *Aerospace Science and Technology*, *91*: 12–17.

Saerens M. and Soquet A.. (1991). Neural controller based on back-propagation algorithm. *Proc. of International Conference on IEE Proceedings F* (Radar and Signal Processing), *138*(1): 55–62.

Stodola P, Kozůbek J and Drozd J. (2018).Using unmanned aerial system in military operations for autonomous reconnaissance. *Proc. of International Conference on Modelling and Simulation for Autonomous Systems*, 514–529.

Wan K, Gao X, Hu Z and Wu G. (2020). Robust Motion Control for UAV in Dynamic Uncertain Environments Using Deep Reinforcement Learning. *Remote Sens*, *12*(4): 640.

Wu B, Han S, Xiao J, Hu X, Fan J. (2016). Error compensation based on s neural network for airborne laser ranging. *Optik-International Journal for Light and Electron Optics*, *127*(8): 4083–4088.

Xiong JJ and Zhang GB. (2016). Global fast dynamic terminal sliding mode control for a quadrotor UAV. *ISA Transactions*, *66*: 233–240.

Yang Y. and Yan Y.. (2016). Attitude regulation for unmanned quadrotors using adaptive fuzzy gain-scheduling sliding mode control. *Aerospace Science and Technology*, *54*: 208–217.

Zheng EH, Xiong JJ and Luo JL. (2014). Second order sliding mode control for a quadrotor UAV. *ISA Transactions*, *53*(4): 1350–1356.

Zulu A. and John S.. (2014). A review of control algorithms for autonomous quadrotors. *Open J. Appl. Sci*, *4*: 547–556.